Supporting Information

Impact of the number of *o*-carboranyl ligands on the photophysical and electroluminescent properties of iridium(III) cyclometalates

Nguyen Van Nghia,[a,†] Sunghee Park,[b,†] Youngjoon An,[a] Junseong Lee,[c] Jaehoon Jung,[a] Seunghyup Yoo,[b,*] and Min Hyung Lee[a,*]

[a] Department of Chemistry and EHSRC, University of Ulsan, Ulsan 44610, Republic of Korea
[b] School of Electrical Engineering, KAIST, Daejeon 34141, Republic of Korea
[c] Department of Chemistry, Chonnam National University, Gwangju 61186, Republic of Korea

Table S1. Crystallographic data and parameters for **3b**–**5b**

	3b ($0.5C_4H_{10}O$)	**4b**	**5b** ($0.5CH_2Cl_2$)·(CH_3OH)
formula	$C_{76}H_{82}B_{20}Ir_2N_6O$	$C_{39}H_{48}B_{20}IrN_3$	$C_{87}H_{130}B_{60}Cl_2Ir_2N_6O_2$
formula weight	1696.07	967.20	2395.86
crystal system	Orthorhombic	Monoclinic	Monoclinic
space group	*Pna*21	*P*2(1)/*c*	*P*2(1)/*c*
a (Å)	9.7157(1)	13.8079(10)	16.4471(3)
b (Å)	23.9775(4)	12.4815(9)	13.8499(2)
c (Å)	16.1910(2)	27.3661(19)	26.5812(4)
α (°)	90	90	90
β (°)	90	104.5200(10)	92.9650(10)
γ (°)	90	90	90
V (Å^3)	3771.83(9)	4565.7(6)	6046.84(17)
Z	2	4	4
ρ_{calc} (g cm^{-3})	1.493	1.407	1.316
μ (mm^{-1})	3.574	2.959	2.289
F(000)	1684	1920	2396
T (K)	100(2)	100(2)	100(2)
scan mode	ϕ and ω	ϕ and ω	ϕ and ω
hkl range	–11→11, –28→21, –19→19	–14→16, –14→14, –32→31	–20→19, –16→16, –32→32
measd reflns	23529	31265	78218
unique reflns [R_{int}]	6609 [0.0513]	7975 [0.0367]	11482 [0.0363]
Reflns used for refinement	6609	7975	11482
refined parameters	499	570	809
R1[a] (I > 2σ(I))	0.0369	0.0258	0.0264
wR2[b] all data	0.0569	0.0673	0.0700
GOF on F^2	1.089	1.031	1.059
ρ_{fin} (max/min) (e Å^{-3})	0.813/–0.957	1.041/–1.559	1.057/–0.391

[a] $R1 = \sum||Fo| - |Fc||/\sum|Fo|$. [b] $wR2 = [\{\sum w(Fo^2 - Fc^2)^2\}/\{\sum w(Fo^2)^2\}]^{1/2}$.

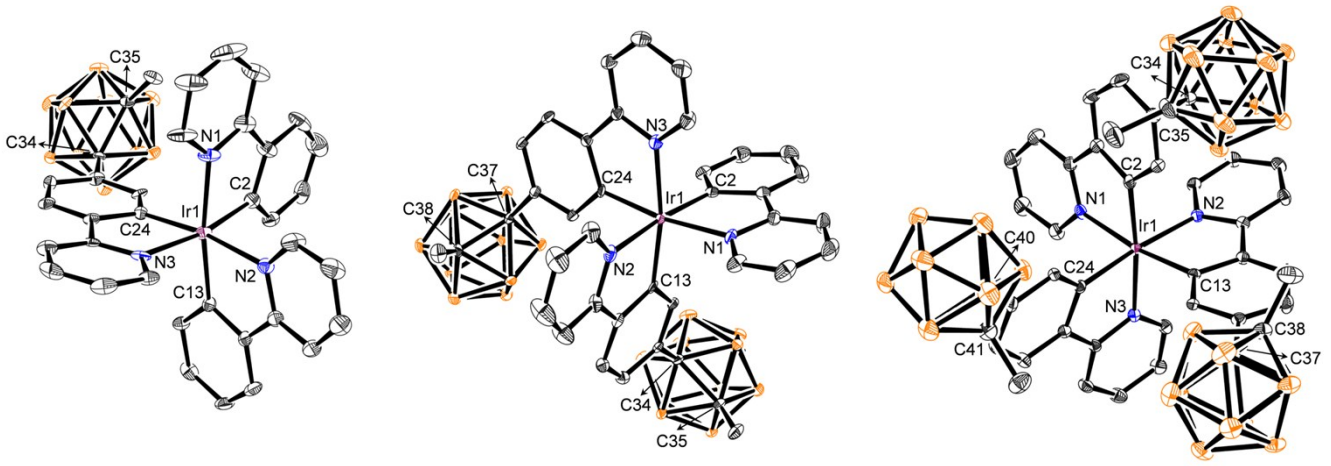

Fig. S1 Crystal structures of **3b**–**5b** (left to right) (40% thermal ellipsoids). H atoms and solvent molecules are omitted for clarity.

Table S2. Selected bond lengths (Å) and angles (deg) for **3b**–**5b**

	3b	**4b**	**5b**
Lengths			
Ir(1)–N(1)	2.127(7)	2.116(3)	2.138(3)
Ir(1)–N(2)	2.136(6)	2.130(2)	2.127(3)
Ir(1)–N(3)	2.138(7)	2.125(2)	2.122(3)
Ir(1)–C(2)	2.014(9)	2.021(3)	2.010(3)
Ir(1)–C(13)	2.024(10)	2.010(2)	2.013(3)
Ir(1)–C(24)	2.001(6)	2.009(3)	2.017(3)
Angles			
C(2)–Ir(1)−N(1)	79.3(3)	79.54(10)	78.82(12)
C(13)–Ir(1)−N(2)	79.5(3)	79.53(9)	79.72(11)
C(24)–Ir(1)−N(3)	79.3(3)	79.60(10)	79.67(11)

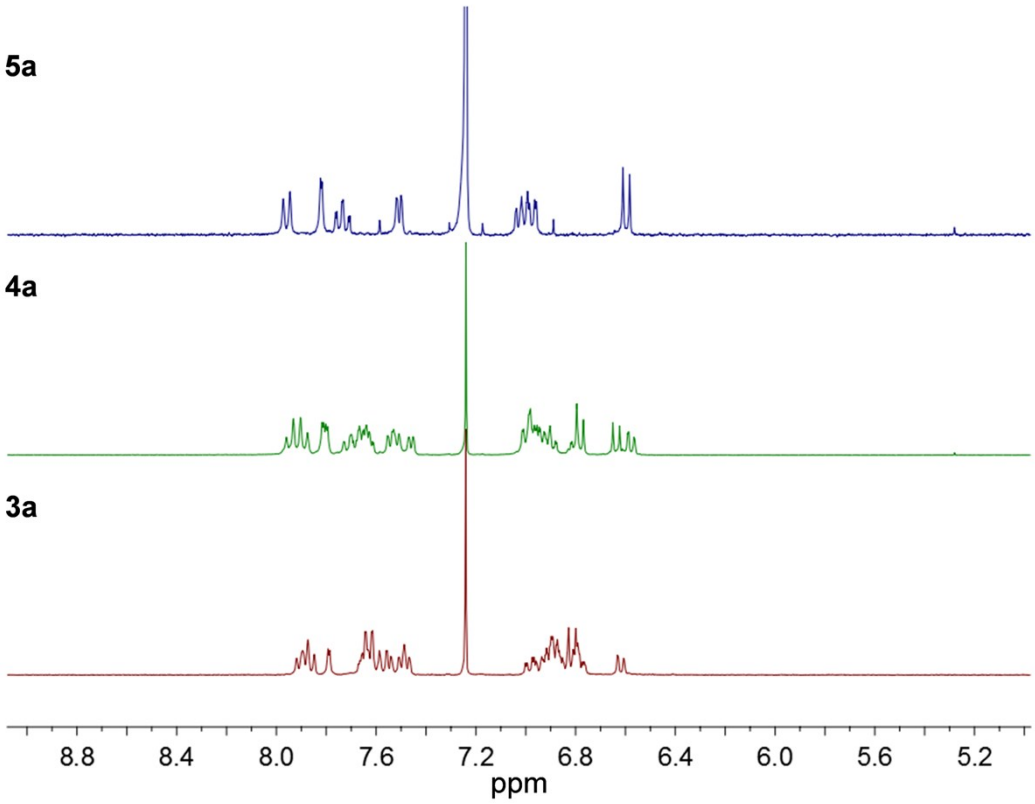

Fig. S2 The aromatic region of the ^{1}H NMR spectra of **3a**–**5a** in $CDCl_3$.

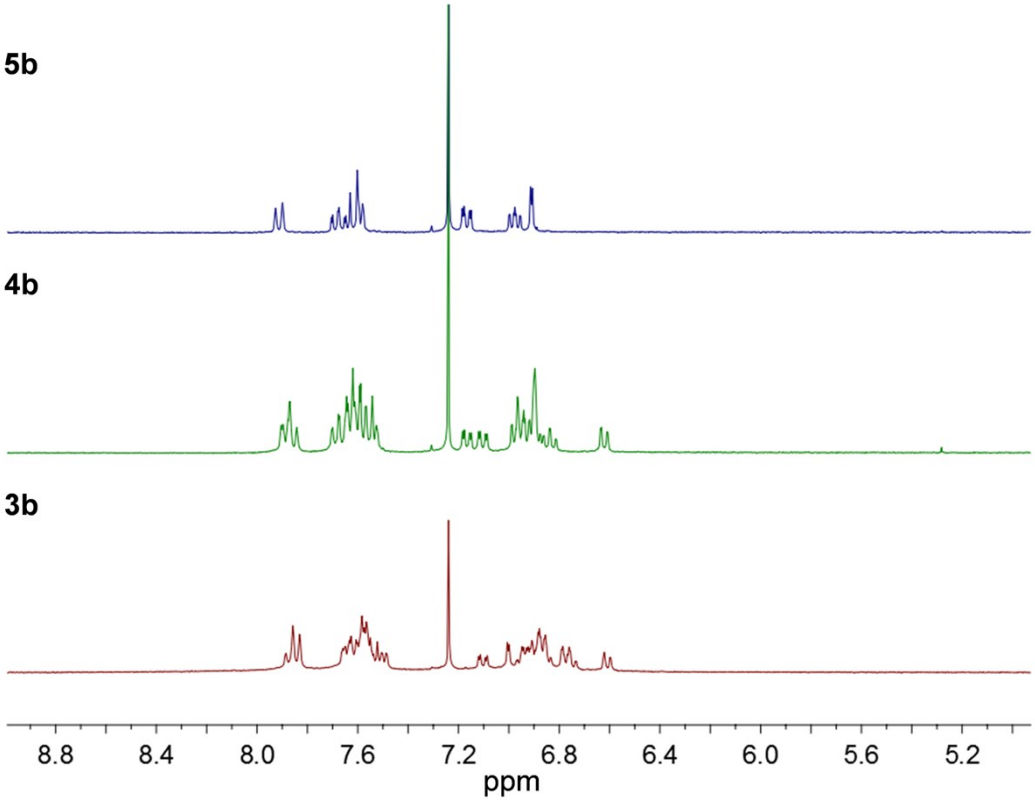

Fig. S3 The aromatic region of the ^{1}H NMR spectra of **3b**–**5b** in $CDCl_3$.

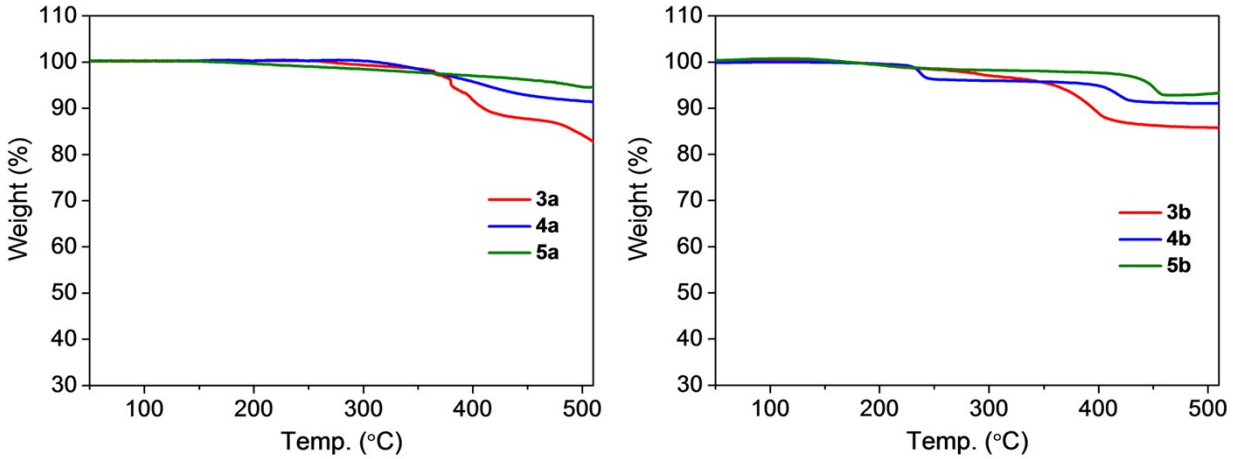

Fig. S4 TGA curves of **3a**–**5a** and **3b**–**5b**.

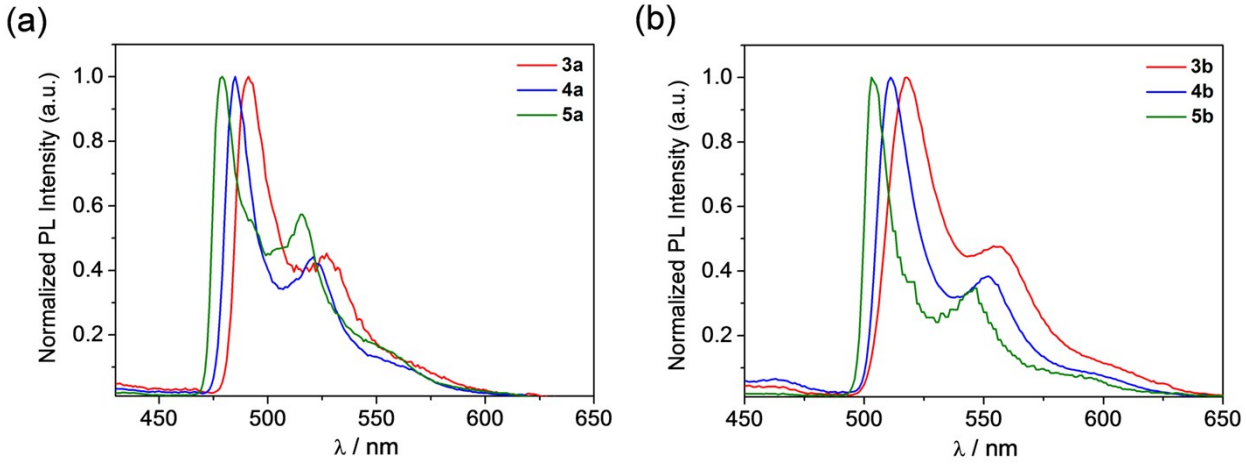

Fig. S5 Normalized PL spectra of **3a**–**5a** and **3b**–**5b** in toluene at 77 K.

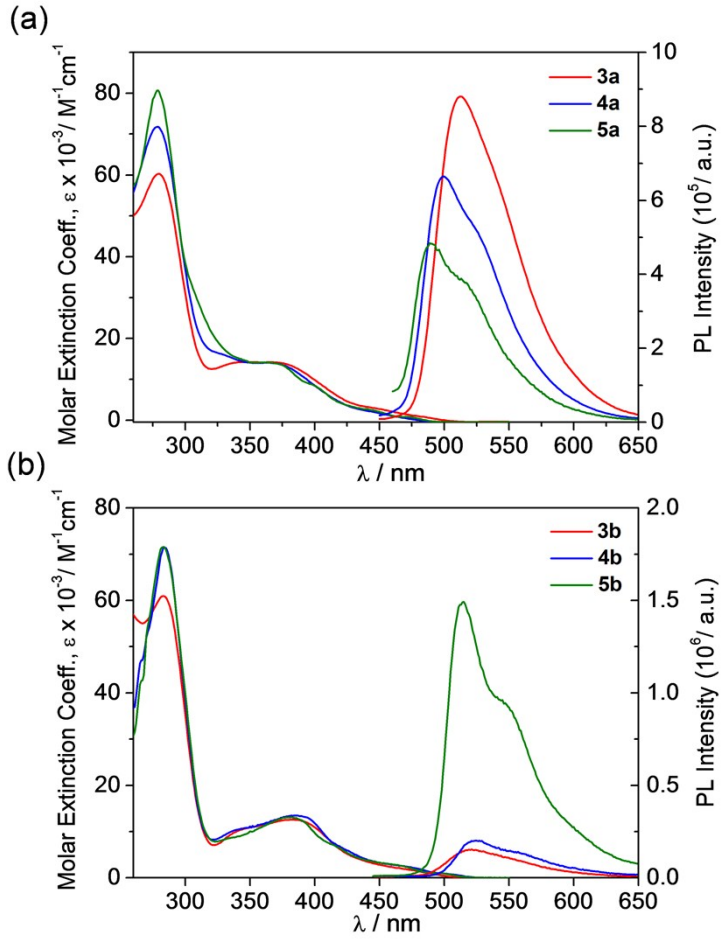

Fig. S6 UV/Vis absorption 5.0 × 10^{-5} M, left) and PL spectra (2.0 × 10^{-5} M, right) of (a) **3a**–**5a** and (b) **3b**–**5b** in THF at 298 K.

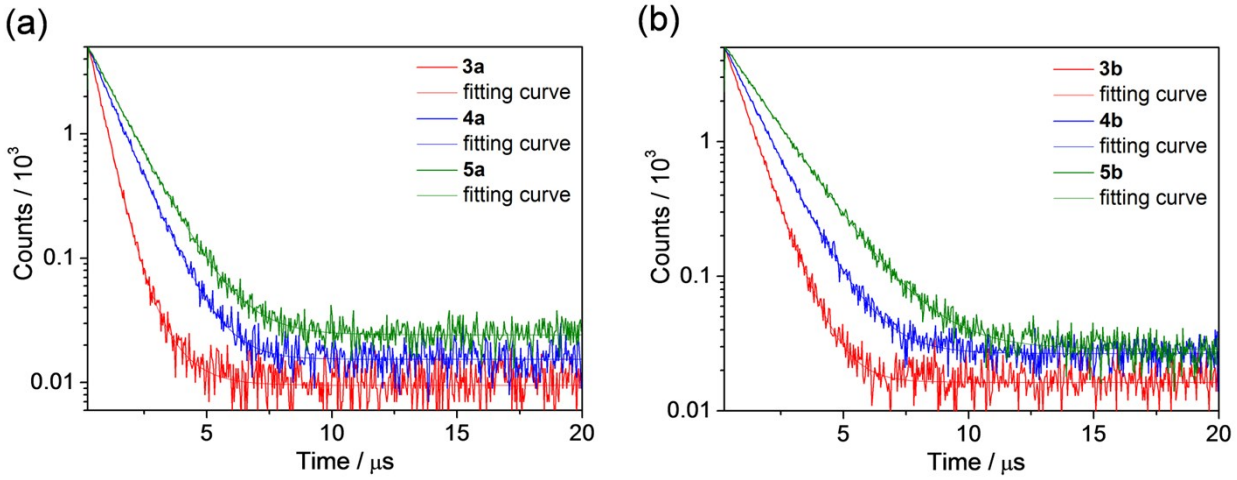

Fig. S7 Emission decay curves of **3a**–**5a** and **3b**–**5b** in toluene at 298 K.

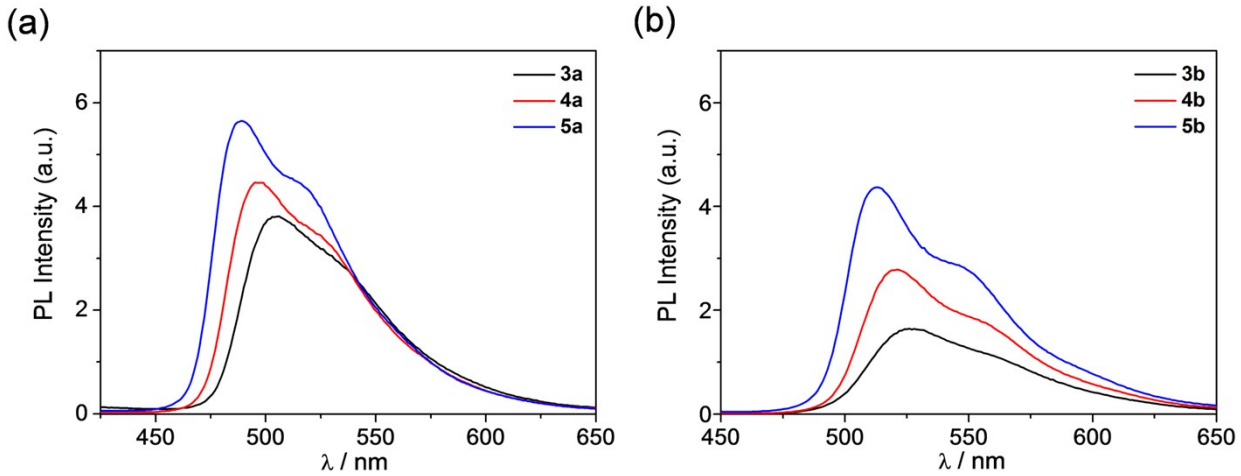

Fig. S8 PL spectra of PMMA film doped with **3a**–**5a** and **3b-5b** (4 wt% of Ir).

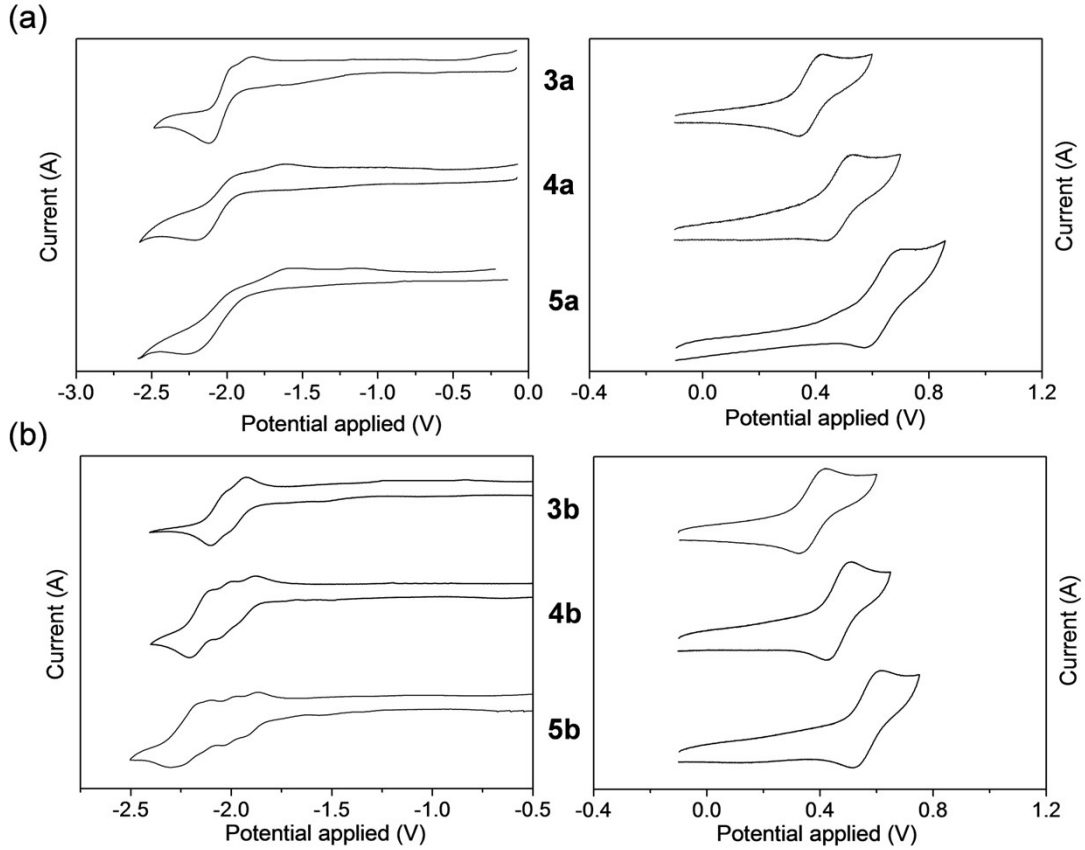

Fig. S9 Cyclic voltammograms of (a) **3a**–**5a** and (b) **3b**–**5b** showing reduction (left) and oxidation (right) (1.0×10^{-3} M in DMF, scan rate = 100–200 mV/s).

DFT computational results

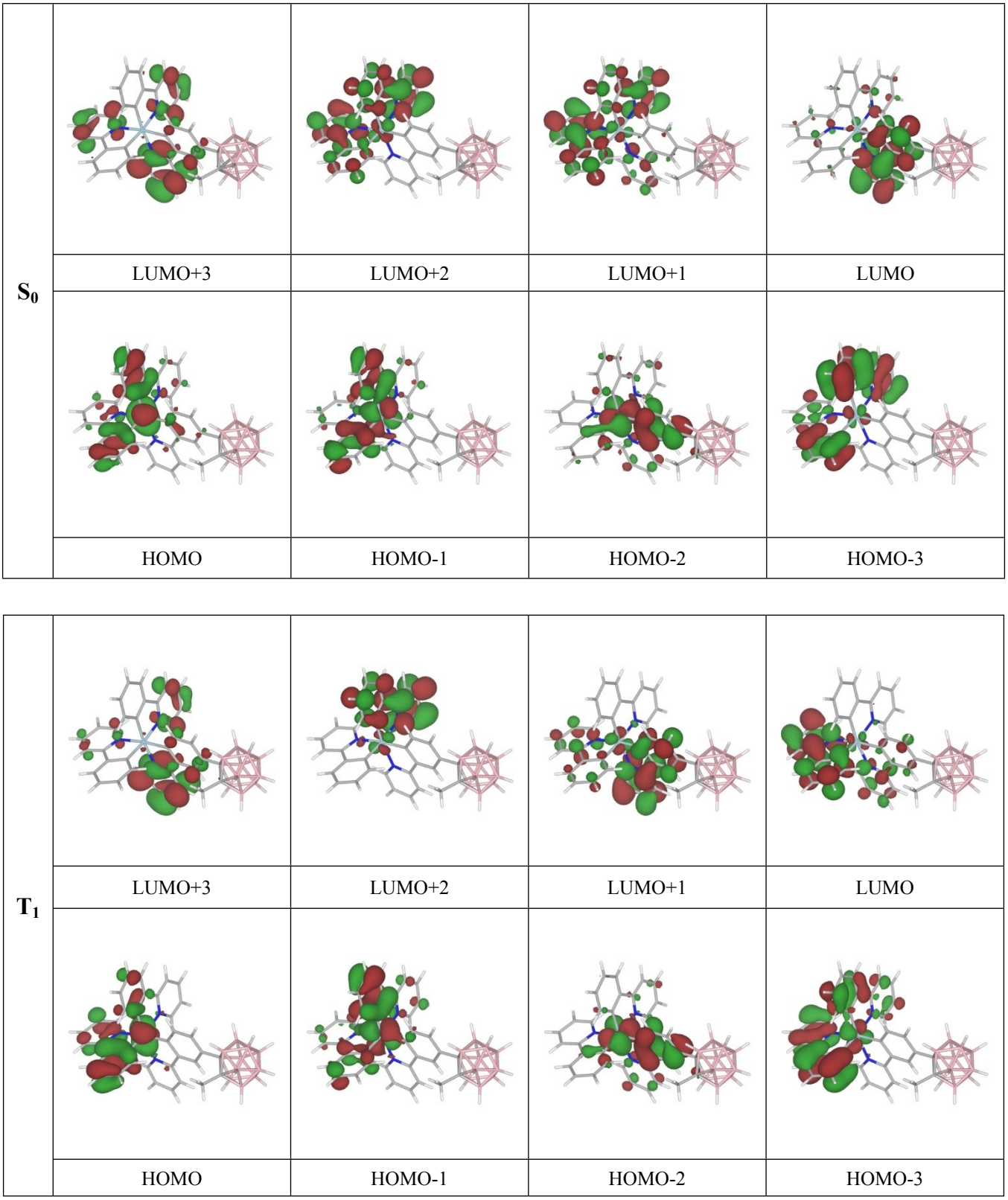

Fig. S10 Molecular orbitals of **3a** optimized by IEFPCM-B3LYP/6-31G(d) calculations (solvent: toluene) for its ground (S_0) and lowest-lying triplet (T_1) states, respectively (Isovalue = 0.03).

Table S3. Molecular orbital energies (in eV) and contributions of moieties (in %) for **3a** at the ground state (S_0) geometry optimized by IEFPCM-B3LYP/6-31G(d) calculation (solvent: toluene). The contributions of MeCB moieties are presented in parentheses.

MO	Energy	Ir	Pyd1	Pyd2	Pyd3	Ph1 (MeCB)	Ph2	Ph3
LUMO+3	-1.09	2.00	49.41	16.78	17.40	8.21(1.94)	2.06	2.21
LUMO+2	-1.31	4.36	0.47	27.51	43.11	0.22(0.04)	9.50	14.79
LUMO+1	-1.36	3.33	7.76	39.00	23.22	2.63(0.10)	14.89	9.07
LUMO	-1.51	2.22	56.78	3.53	4.35	27.90(1.03)	2.09	2.09
HOMO	-5.21	48.80	1.80	4.03	3.33	3.98(0.22)	16.69	21.14
HOMO-1	-5.30	41.19	2.24	4.74	3.35	1.47(0.01)	24.56	22.45
HOMO-2	-5.43	46.73	5.11	1.31	3.91	31.19(2.83)	5.27	3.65
HOMO-3	-6.12	3.46	0.53	7.42	17.67	0.94(0.08)	23.54	46.37

Table S4. Molecular orbital energies (in eV) and contributions of moieties (in %) for **3a** at the lowest-lying triplet state (T_1) geometry optimized by IEFPCM-B3LYP/6-31G(d) calculation (solvent: toluene). The contributions of MeCB moieties are presented in parentheses.

MO	Energy	Ir	Pyd1	Pyd2	Pyd3	Ph1 (MeCB)	Ph2	Ph3
LUMO+3	-1.08	1.92	62.42	6.01	14.52	10.31(2.29)	0.80	1.72
LUMO+2	-1.32	3.43	0.74	1.44	68.56	0.30(0.03)	0.56	24.94
LUMO+1	-1.51	4.22	53.69	10.06	0.68	24.96(0.92)	5.22	0.24
LUMO	-1.64	2.62	10.63	48.87	1.65	5.40(0.19)	29.44	1.21
HOMO	-5.09	41.65	1.94	10.67	1.49	1.47(0.04)	32.13	10.61
HOMO-1	-5.30	39.04	1.30	5.88	4.88	2.44(0.04)	13.31	33.11
HOMO-2	-5.48	48.43	5.15	1.07	3.41	32.67(2.91)	3.88	2.48
HOMO-3	-6.07	9.39	1.15	20.47	6.64	0.90(0.05)	46.30	15.12

Table S5. Computed absorption and phosphorescence emission wavelengths (λ_{calc} in nm) and contributions of metal-to-ligand charge transfer (MLCT, in %) to the transition for **3a** from IEFPCM-TD-B3LYP/6-31G(d) calculations at the ground (S_0) and lowest-lying triplet state (T_1) optimized geometries, respectively.

State	$\lambda_{calc.}$ / nm	$f_{calc.}$	Major contribution	MLCT(%)
S_1	421.9	0.0037	HOMO → LUMO (94%)	46.58
S_2	404.7	0.0129	HOMO → LUMO+1 (90%)	45.47
S_3	402.1	0.0221	HOMO-1 → LUMO (75%)	38.97
			HOMO → LUMO+2 (13%)	44.44
S_4	398.8	0.0014	HOMO → LUMO+2 (79%)	44.44
			HOMO-1 → LUMO (14%)	38.97
S_5	385.5	0.0844	HOMO-2 → LUMO (63%)	44.51
			HOMO-1 → LUMO+1 (23%)	37.86
S_6	381.4	0.0553	HOMO-1 → LUMO+1 (44%)	37.86
			HOMO-1 → LUMO+2 (27%)	36.83
			HOMO-2 → LUMO (24%)	44.51
T_1	503.0[a]	0.0000	HOMO → LUMO (70%)	39.03
			HOMO → LUMO+1 (10%)	37.43

[a] For the adiabatic transition corresponding to the 0−0 phosphorescence.

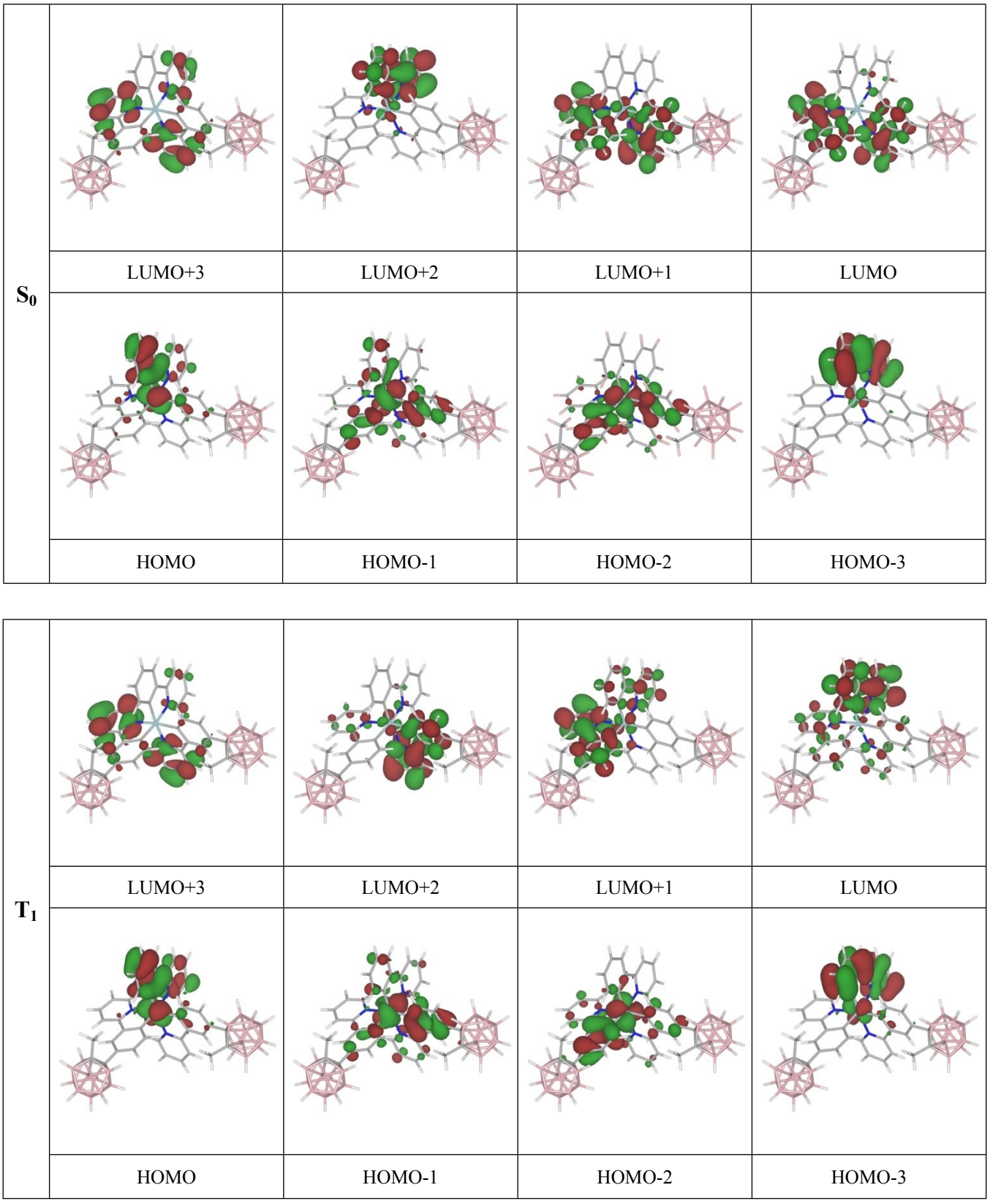

Fig. S11 Molecular orbitals of **4a** optimized by IEFPCM-B3LYP/6-31G(d) calculations (solvent: toluene) for its ground (S_0) and lowest-lying triplet (T_1) states, respectively (Isovalue = 0.03).

Table S6. Molecular orbital energies (in eV) and contributions of moieties (in %) for **4a** at the ground state (S_0) geometry optimized by IEFPCM-B3LYP/6-31G(d) calculation (solvent: toluene). The contributions of MeCB moieties are presented in parentheses.

MO	Energy	Ir	Pyd1	Pyd2	Pyd3	Ph1 (MeCB)	Ph2 (MeCB)	Ph3
LUMO+3	-1.25	1.81	34.81	33.05	14.38	5.73(1.12)	5.96(1.25)	1.87
LUMO+2	-1.48	3.81	2.32	1.95	66.23	0.83(0.06)	0.58(0.02)	24.20
LUMO+1	-1.60	4.28	34.59	30.77	0.43	15.17(0.55)	13.56(0.48)	0.17
LUMO	-1.69	1.59	28.26	31.64	3.56	14.63(0.52)	17.09(0.68)	2.03
HOMO	-5.43	46.21	1.07	2.93	5.63	4.87(0.25)	2.98(0.19)	35.89
HOMO-1	-5.59	46.01	4.19	3.01	2.87	15.40(1.25)	15.07(1.30)	10.90
HOMO-2	-5.66	44.82	4.71	3.52	2.47	18.37(1.70)	20.43(1.71)	2.28
HOMO-3	-6.29	3.67	1.02	0.54	23.90	2.09(0.11)	0.84(0.02)	67.81

Table S7. Molecular orbital energies (in eV) and contributions of moieties (in %) for **4a** at the lowest-lying triplet state (T_1) geometry optimized by IEFPCM-B3LYP/6-31G(d) calculation (solvent: toluene). The contributions of MeCB moieties are presented in parentheses.

MO	Energy	Ir	Pyd1	Pyd2	Pyd3	Ph1 (MeCB)	Ph2 (MeCB)	Ph3
LUMO+3	-1.24	1.74	32.96	43.07	6.24	5.11(1.01)	7.60(1.50)	0.78
LUMO+2	-1.60	3.72	57.04	5.39	3.09	26.11(0.92)	2.11(0.07)	1.55
LUMO+1	-1.65	4.18	2.23	49.00	12.40	1.06(0.04)	23.60(0.90)	6.59
LUMO	-1.79	2.13	5.91	10.12	44.51	3.95(0.16)	5.39(0.20)	27.62
HOMO	-5.29	37.09	0.66	2.20	13.44	4.20(0.21)	0.91(0.03)	41.26
HOMO-1	-5.61	45.66	4.85	1.81	4.27	24.17(2.06)	9.18(0.66)	7.34
HOMO-2	-5.69	45.75	3.74	4.72	1.75	9.09(0.84)	28.46(2.47)	3.19
HOMO-3	-6.23	11.31	1.28	1.49	24.78	3.50(0.19)	1.31(0.03)	56.10

Table S8. Computed absorption and phosphorescence emission wavelengths (λ_{calc} in nm) and contributions of metal-to-ligand charge transfer (MLCT, in %) to the transition for **4a** from IEFPCM-TD-B3LYP/6-31G(d) calculations at the ground (S_0) and lowest-lying triplet state (T_1) optimized geometries, respectively.

State	$\lambda_{calc.}$ / nm	$f_{calc.}$	Major contribution	MLCT(%)
S_1	411.4	0.0063	HOMO → LUMO (91%)	44.62
S_2	404.7	0.0021	HOMO → LUMO+1 (90%)	41.93
S_3	390.9	0.0365	HOMO → LUMO+2 (68%)	42.40
			HOMO-1 → LUMO (25%)	44.42
S_4	388.2	0.0179	HOMO-1 → LUMO (57%)	44.42
			HOMO → LUMO+2 (25%)	42.40
			HOMO-1 → LUMO+1 (12%)	41.73
S_5	381.1	0.0045	HOMO-1 → LUMO+1 (58%)	41.73
			HOMO-2 → LUMO (18%)	43.23
S_6	378.0	0.1135	HOMO-2 → LUMO (74%)	43.23
			HOMO-1 → LUMO+1 (16%)	41.73
T_1	498.3[a]	0.0000	HOMO → LUMO (69%)	34.96
			HOMO → LUMO+1 (14%)	34.09

[a] For the adiabatic transition corresponding to the 0−0 phosphorescence.

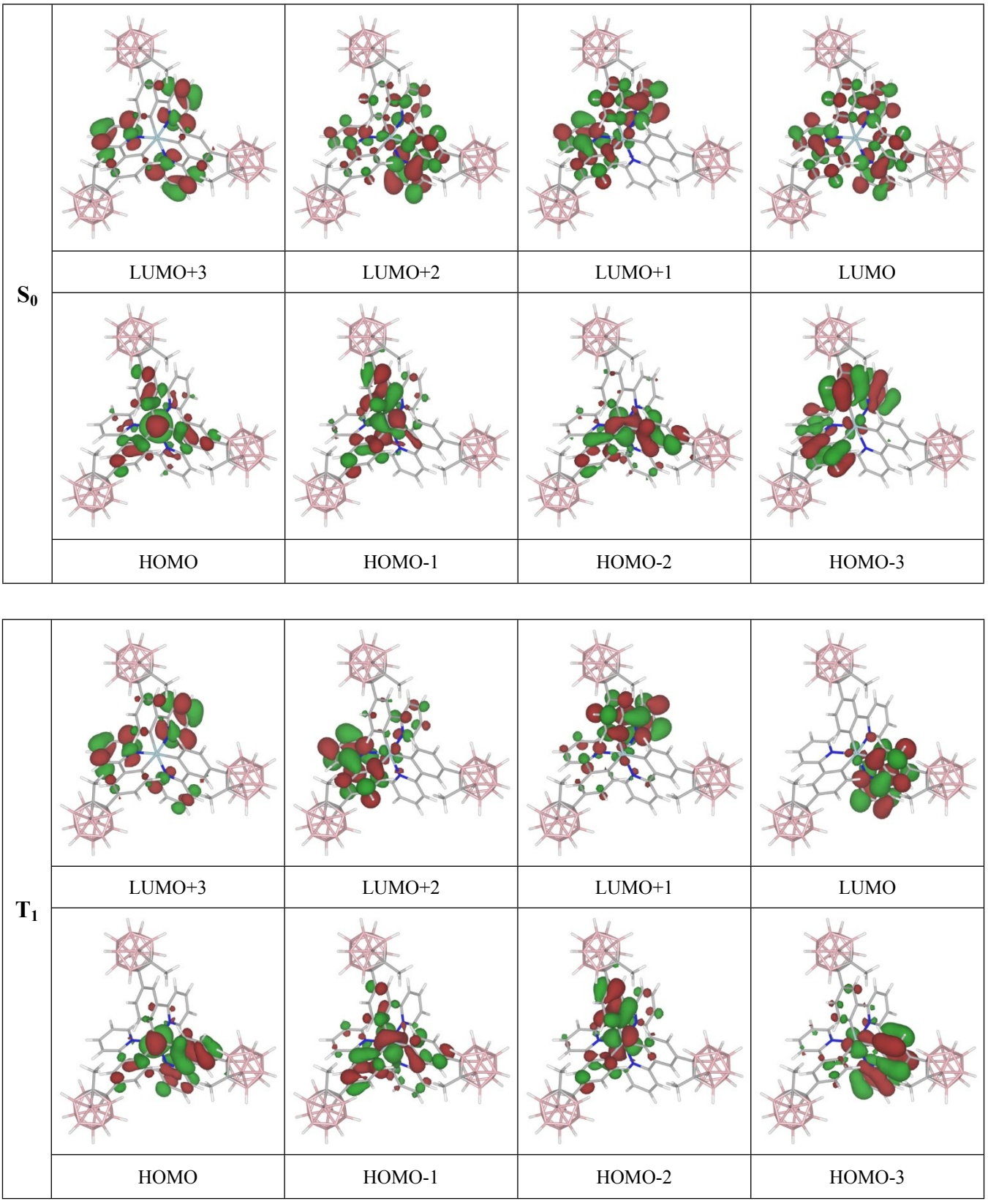

Fig. S12 Molecular orbitals of **5a** optimized by IEFPCM-B3LYP/6-31G(d) calculations (solvent: toluene) for its ground (S_0) and lowest-lying triplet (T_1) states, respectively (Isovalue = 0.03).

Table S9. Molecular orbital energies (in eV) and contributions of moieties (in %) for **5a** at the ground state (S_0) geometry optimized by IEFPCM-B3LYP/6-31G(d) calculation (solvent: toluene). The contributions of MeCB moieties are presented in parentheses.

MO	Energy	Ir	Pyd1	Pyd2	Pyd3	Ph1 (MeCB)	Ph2 (MeCB)	Ph3 (MeCB)
LUMO+3	-1.41	1.65	28.15	26.48	26.62	5.09(0.96)	4.57(0.79)	4.79(0.89)
LUMO+2	-1.73	4.18	40.96	12.77	12.03	17.86(0.61)	5.62(0.19)	5.57(0.22)
LUMO+1	-1.74	4.17	0.35	32.02	33.12	0.14(0.01)	14.50(0.54)	14.65(0.49)
LUMO	-1.84	1.16	23.50	19.65	19.40	13.03(0.47)	11.03(0.42)	10.94(0.40)
HOMO	-5.71	51.08	3.12	3.16	3.14	12.01(0.94)	12.29(0.96)	12.35(0.96)
HOMO-1	-5.84	43.25	2.23	4.29	4.26	3.53(0.13)	14.01(1.31)	24.84(2.15)
HOMO-2	-5.84	43.19	5.03	2.92	2.94	24.78(2.26)	14.23(1.09)	3.34(0.23)
HOMO-3	-6.66	4.35	1.64	10.35	18.39	1.91(0.08)	25.47(0.25)	37.19(0.37)

Table S10. Molecular orbital energies (in eV) and contributions of moieties (in %) for **5a** at the lowest-lying triplet state (T_1) geometry optimized by IEFPCM-B3LYP/6-31G(d) calculation (solvent: toluene). The contributions of MeCB moieties are presented in parentheses.

MO	Energy	Ir	Pyd1	Pyd2	Pyd3	Ph1 (MeCB)	Ph2 (MeCB)	Ph3 (MeCB)
LUMO+3	-1.37	1.67	11.55	30.87	38.88	2.40(0.54)	4.97(0.86)	7.03(1.25)
LUMO+2	-1.74	3.63	0.88	55.30	8.90	0.37(0.01)	26.23(0.96)	3.62(0.12)
LUMO+1	-1.79	3.11	2.69	7.91	53.42	1.31(0.06)	4.13(0.14)	26.26(0.95)
LUMO	-2.10	3.04	52.68	1.32	2.30	37.02(1.09)	1.29(0.06)	1.17(0.04)
HOMO	-5.62	43.66	11.02	1.62	2.17	26.34(1.90)	9.53(0.71)	2.91(0.15)
HOMO-1	-5.84	40.88	6.35	4.21	2.44	14.43(1.20)	18.87(1.54)	9.34(0.74)
HOMO-2	-5.87	43.75	1.72	3.79	4.90	2.60(0.04)	11.09(1.04)	28.62(2.45)
HOMO-3	-6.56	12.65	25.24	2.70	2.85	45.99(0.52)	4.97(0.17)	4.83(0.08)

Table S11. Computed absorption and phosphorescence emission wavelengths (λ_{calc} in nm) and contributions of metal-to-ligand charge transfer (MLCT, in %) to the transition for **5a** from IEFPCM-TD-B3LYP/6-31G(d) calculations at the ground (S_0) and lowest-lying triplet state (T_1) optimized geometries, respectively.

State	$\lambda_{calc.}$ / nm	$f_{calc.}$	Major contribution	MLCT(%)
S_1	397.7	0.0088	HOMO → LUMO (97%)	49.92
S_2	390.1	0.0056	HOMO → LUMO+1 (95%)	46.91
S_3	389.9	0.0056	HOMO → LUMO+2 (95%)	46.90
S_4	375.0	0.0560	HOMO-1 → LUMO (91%)	42.09
S_5	374.2	0.0636	HOMO-2 → LUMO (91%)	42.03
S_6	370.3	0.0058	HOMO-1 → LUMO+2 (44%)	39.07
			HOMO-2 → LUMO+1 (42%)	39.02
T_1	489.9[a]	0.0000	HOMO → LUMO (73%)	40.62
			HOMO-3 → LUMO (12%)	9.61

[a] For the adiabatic transition corresponding to the 0−0 phosphorescence.

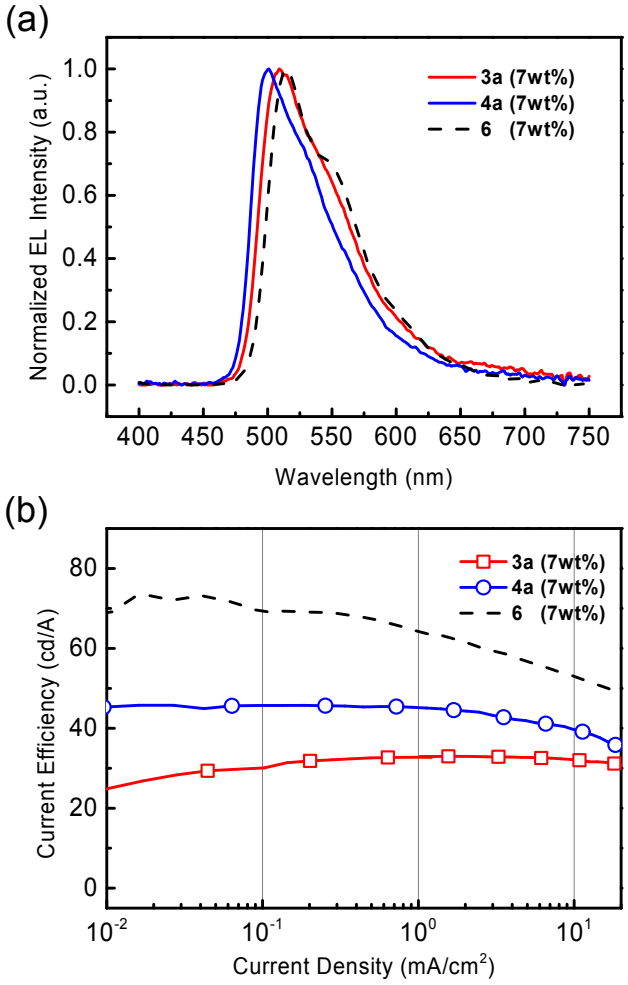

Fig. S13 (a) EL spectra of devices (**D3-II**, **D4-II**, and **D6-II**) fabricated with CBP host doped with **3a**, **4a**, and **6** at 7 wt% as an emitter, and (b) current efficiency–current density (η_{CE}–J) curves.

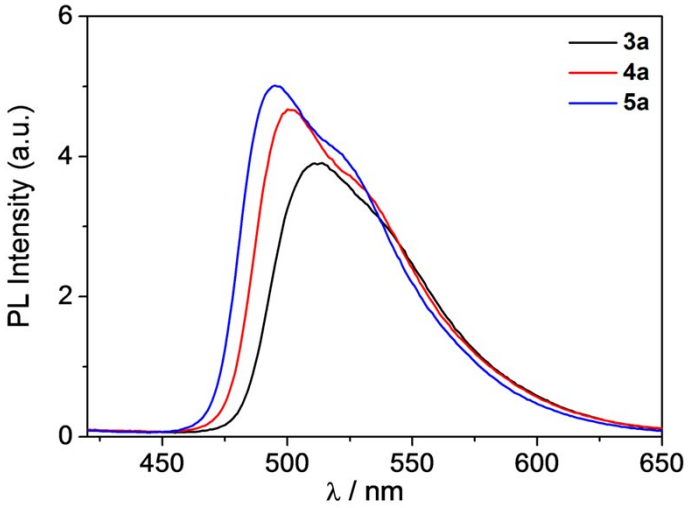

	λ_{PL} (nm)	Φ_{PL} (%)
3a	512	29 (±0.58)
4a	501	31 (±0.0)
5a	496	32 (±0.58)

Fig. S14 PL spectra and absolute PLQYs of PNB-CBP film doped with **3a**–**5a** (8 wt% of Ir).

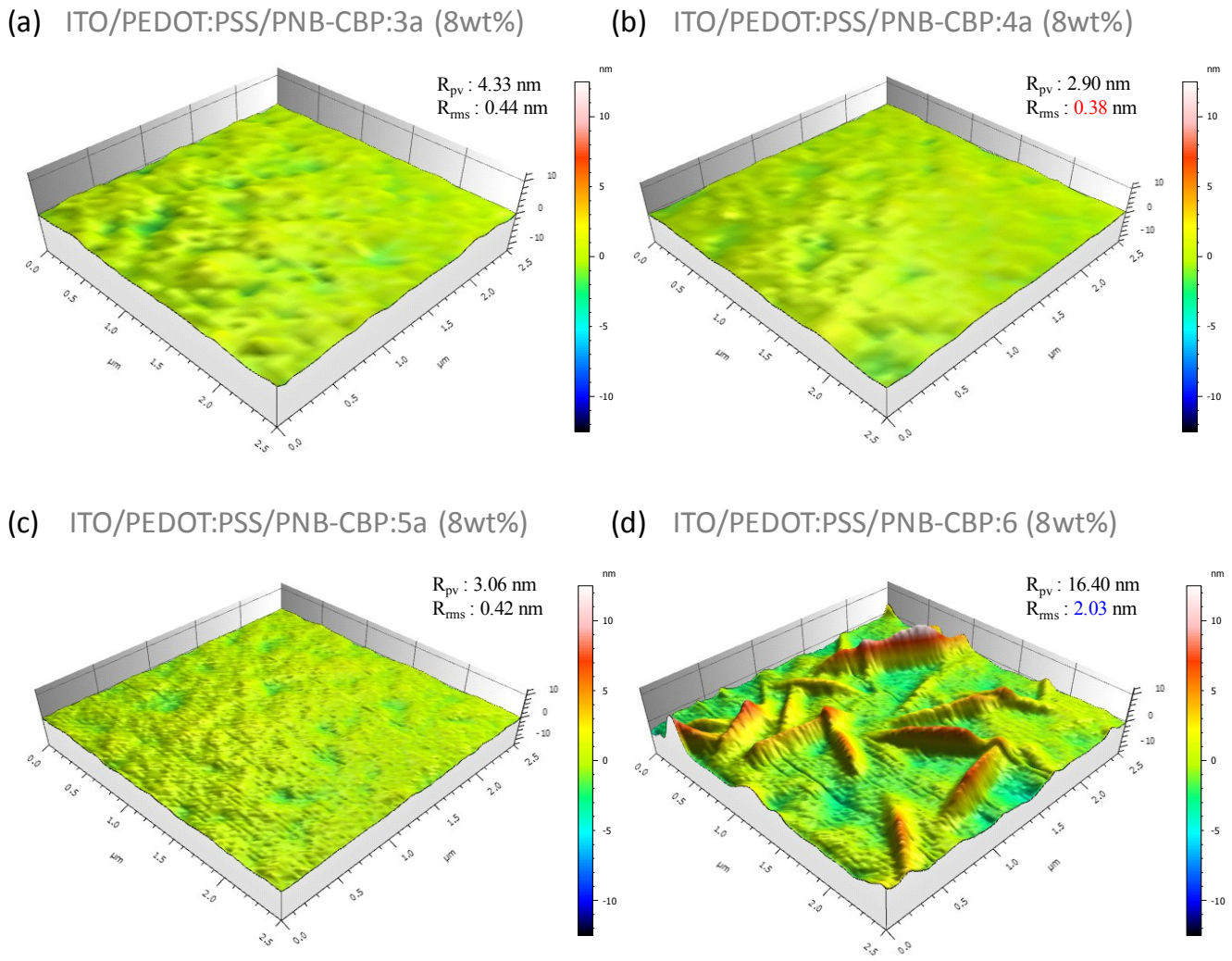

Fig. S15 Atomic force microscope (AFM) images of 2.5 µm × 2.5 µm area of spin-coated PNB-CBP films on ITO/PEDOT:PSS (AI4083) substrates doped with (a) **3a**, (b) **4a**, (c) **5a**, and (d) **6** at 8 wt%.